CMS Physics Analysis Summary

Contact: cms-pag-conveners-susy@cern.ch 2016/03/21

Search for supersymmetry in events with one lepton in proton-proton collisions at $\sqrt{s}$=13 TeV with the CMS experiment

The CMS Collaboration

Abstract

A search for supersymmetry in events with a single electron or muon is performed on proton-proton collision data with the CMS experiment at a center-of-mass energy of 13 TeV, in a dataset corresponding to an integrated luminosity of 2.3 fb^{-1}. Several exclusive search regions are defined, based on the number of b-tagged jets, the scalar sum of all jet transverse momenta, and the scalar sum of the transverse missing momentum and transverse lepton momentum. The observed yields are compatible with predictions from standard model processes. The results are interpreted in two simplified models describing gluino pair production. In a model where each gluino decays to top quarks and a neutralino, gluinos with masses up to 1.575 TeV are excluded for neutralino masses below 600 GeV. In the second model, each gluino decays to two light quarks and an intermediate chargino, with the latter decaying to a W boson and a neutralino. Here, gluino masses below 1.4 TeV are excluded for neutralino masses below 725 GeV, assuming a chargino with mass midway between the gluino and neutralino mass.

1 Introduction

An inclusive search for supersymmetry (SUSY) in the single-lepton channel has been performed with 13 TeV data taken in 2015 with the CMS experiment, corresponding to an integrated luminosity of 2.3 fb^{-1}. Similar searches have been performed on 7 TeV data [1–3] and on 8 TeV data [4–6] by the CMS and ATLAS collaborations. First results of searches in the single lepton final state at 13 TeV are available as well [7–9]. In this note, a search for gluino pair production is presented in signal regions with and without b-tag requirements in order to be sensitive to a large variety of SUSY models. Exclusive search regions are characterized by the number of jets, the number of b-tagged jets, the scalar sum of the transverse momenta (p_T) of the jets (H_T), and the scalar sum of the lepton p_T and the missing transverse energy (L_T).

For the background estimation a method similar to the one described in [4] as the "R_CS method" is used, exploiting the fact that the main backgrounds are $\text{t}\bar{\text{t}}$ and W + jets events, with one W boson decaying leptonically. The W-boson candidate p_T is reconstructed as the vector sum of the lepton p_T and the missing transverse momentum vector (p_T^miss). The latter is defined as the negative vector sum of all reconstructed objects and its magnitude is referred to as missing transverse energy E_T^miss. The azimuthal angle $\Delta\Phi$ between the W-boson candidate and the lepton is used to separate the signal from the background: For W + jets and semileptonic $\text{t}\bar{\text{t}}$ events $\Delta\Phi$ has a maximum value, which is fixed by the mass of the W boson and its momentum. Conversely, in SUSY the E_T^miss is not only caused by the neutrino from the W boson decay, but also from the lightest SUSY particle (LSP), leading to a nearly uniform distribution of the $\Delta\Phi$ values. Therefore, the main backgrounds can be suppressed by rejecting events with a small $\Delta\Phi$ angle. Other backgrounds, like $\text{t}\bar{\text{t}}$ events where both W bosons decay to a lepton and a neutrino, and one lepton is out of acceptance or not identified, also populate the high $\Delta\Phi$ region. Since gluino-gluino production leads to final states with a large number of jets, the signal-to-background ratio is very small in regions with a low number of jets, which is used here to determine the normalization of the background without large signal contamination. The QCD background is estimated separately.

Depending on the signal model, the signal regions have varying sensitivity. This search focuses on gluino-gluino production in the T1t^4 model (Fig. 1, left) and the $\text{T5q}^4\text{WW}$ model (Fig. 1, right). In T1t^4, pair-produced gluinos each decay to a top-antitop pair ($\text{t}\bar{\text{t}}$) and the lightest neutralino ($\widetilde{\chi}_1^0$). In $\text{T5q}^4\text{WW}$, the pair-produced gluinos each decay to a quark-antiquark pair of the first or second generation ($\text{q}\bar{\text{q}}$), and a chargino ($\widetilde{\chi}_1^\pm$) with its mass defined as $m_{\widetilde{\chi}_1^\pm} = 0.5(m_{\widetilde{\text{g}}} + m_{\widetilde{\chi}_1^0})$. This chargino then decays to a W boson and the $\widetilde{\chi}_1^0$, where the W boson can be virtual, depending on the mass difference between the chargino and the lightest neutralino.

The organization of this document is as follows. In Section 2 the CMS detector is described. In Section 3 the event reconstruction and in Section 4 the event selection are discussed. The background estimation with the R_CS method as well as the QCD background estimation are given in Section 5. An overview of the main systematic uncertainties is presented in Section 6. The results are discussed and interpreted in Section 7, and a summary is given in Section 8.

2 The CMS detector

The central feature of the CMS apparatus is a superconducting solenoid of 6 m internal diameter, providing a magnetic field of 3.8 T. Within the superconducting solenoid volume are a silicon pixel and strip tracker, a lead tungstate crystal electromagnetic calorimeter (ECAL), and a brass and scintillator hadron calorimeter (HCAL), each composed of a barrel and two endcap

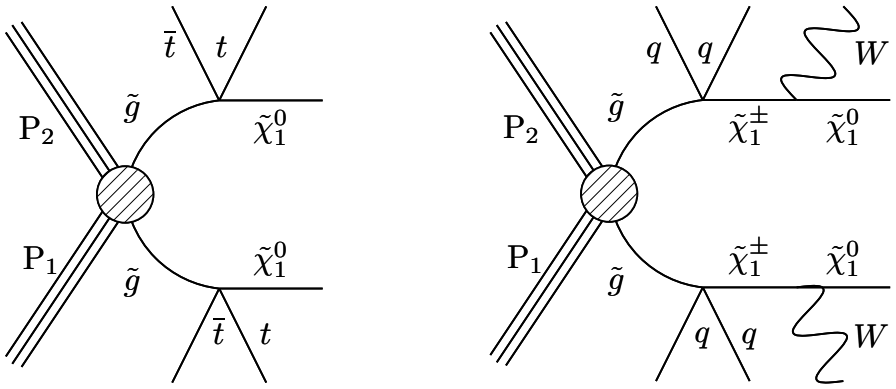

Figure 1: Graphs showing the simplified models T1t^4 (left) and T5q^{4}WW (right). Depending on the mass difference between the chargino ($\tilde{\chi}_1^\pm$) and the neutralino ($\tilde{\chi}_1^0$), the W boson can be virtual.

sections. Forward calorimeters extend the pseudorapidity [10] coverage provided by the barrel and endcap detectors. Muons are measured in gas-ionization detectors embedded in the steel flux-return yoke outside the solenoid.

The silicon tracker measures charged particles within the pseudorapidity range $|\eta| < 2.5$. Isolated particles of a transverse momentum p_T = 100 GeV emitted at $|\eta| < 1.4$ have track resolutions of 2.8% in p_T and 10 (30) μm in the transverse (longitudinal) impact parameter [11]. The ECAL and HCAL measure energy deposits in the pseudorapidity range $|\eta| < 3$, with quartz-steel forward calorimeters extending the coverage to $|\eta| < 5$. When combining information from the entire detector, the jet energy resolution amounts typically to 15% at 10 GeV, 8% at 100 GeV, and 4% at 1 TeV. The electron momentum is estimated by combining the energy measurement in the ECAL with the momentum measurement in the tracker. The momentum resolution for electrons with $p_T \approx 45$ GeV from $Z \to ee$ decays ranges from 1.7% for nonshowering electrons in the barrel region to 4.5% for showering electrons in the endcaps [12]. Muons are measured in the pseudorapidity range $|\eta| < 2.4$, with detection planes made using three technologies: drift tubes, cathode strip chambers, and resistive plate chambers. Matching muons to tracks measured in the silicon tracker results in a relative transverse momentum resolution for muons with $20 < p_T < 100$ GeV of 1.3–2.0% in the barrel and better than 6% in the endcaps, The p_T resolution in the barrel is better than 10% for muons with p_T up to 1 TeV [13].

The CMS trigger system consists of two levels, where the first level (L1), composed of custom hardware processors, uses information from the calorimeters and muon detectors to select the most interesting events in a fixed time interval of less than 4 μs. The high-level trigger (HLT) processor farm further decreases the event rate from around 100 kHz to less than 1 kHz, before data storage.

A more detailed description of the CMS detector, together with a definition of the coordinate system used and the relevant kinematic variables, can be found in Ref. [10].

3 Event reconstruction

All objects in the event are reconstructed with the particle-flow event algorithm [14, 15] which reconstructs and identifies each individual particle with an optimized combination of information from the various elements of the CMS detector. The energy of electrons is determined from a combination of the electron momentum at the primary interaction vertex as deter-

mined by the tracker, the energy of the corresponding ECAL cluster, and the energy sum of all bremsstrahlung photons spatially compatible with originating from the electron track [12]. Electron candidates are required to satisfy identification criteria in order to suppress contributions from misidentified jets, photon conversions, and electrons from heavy flavor decays. In this analysis, a 'tight' electron ID working point with an efficiency of about 70% is used for the signal selection, a 'medium' working point with an efficiency of about 80% for the estimation of the QCD background, and a 'veto' working point with an average efficiency of 95%. Muons are reconstructed from a stand-alone muon track from the muon system serving as a seed to find a corresponding silicon track [13]. The energy of charged hadrons is determined from a combination of their momentum measured in the tracker and the matching ECAL and HCAL energy deposits, corrected for zero-suppression effects and for the response function of the calorimeters to hadronic showers. Finally, the energy of neutral hadrons is obtained from the corresponding corrected ECAL and HCAL energy.

Jets are clustered with the anti-k_t algorithm with a distance parameter R of 0.4 [16]. Jet momentum is determined as the vectorial sum of all particle momenta in the jet, and is found from simulation to be within 5% to 10% of the true momentum over the whole p_T spectrum and detector acceptance. An offset correction is applied to jet energies to take into account the contribution from additional (pileup) proton-proton interactions within the same bunch crossing [17]. Jet energy corrections are derived from simulation, and are confirmed with in situ measurements of the energy balance in dijet and photon+jet events [16]. Additional selection criteria are applied to each event to remove spurious jet-like features originating from isolated noise patterns in certain HCAL regions. Jets are selected with $p_T > 30\,\text{GeV}$ and $|\eta| < 2.4$. All signal regions require at least five jets.

To discriminate jets originating from b-quarks, the inclusive combined secondary vertex (CSV) tagger [18, 19] which contains both secondary vertex and track-based information. A working point with about 70% b-tagging efficiency and 1.5% light-flavor misidentification rate is chosen [20]. Depending on the targeted signal, the search regions are defined to contain either zero b-tagged jets (called in the following 'zero-b'), or at least one b-tagged jet (called 'multi-b').

The electron or muon candidate is required to have a minimum p_T of 25 GeV, while 'veto' leptons are selected with loosened identification criteria and a minimum p_T of 10 GeV. An isolation variable is defined as the p_T sum of all objects within a cone around the lepton candidate (excluding the candidate itself), describing the activity around the object. An area correction is applied in order to remove the pileup contribution. This analysis uses an isolation in a p_T-dependent cone around the lepton: for $p_T < 50\,\text{GeV}$, $R = 0.2$; for $50\,\text{GeV} < p_T < 200\,\text{GeV}$, $R = 10\,\text{GeV} / p_T\,[\text{GeV}]$; and for $p_T > 200\,\text{GeV}$, $R = 0.05$. The isolation variable is then divided by the lepton p_T and a common requirement on this relative isolation of < 0.4 is applied for all veto leptons, whereas selected muons and electrons have to satisfy 0.2 and 0.1, respectively. The use of the lepton-p_T dependent isolation cone enhances the acceptance of signal events containing a large amount of hadronic energy.

Double counting of objects is avoided by not considering jet objects if they lie within a cone of 0.4 around a lepton. At the analysis level, events are selected if they contain exactly one lepton and no veto leptons.

4 Trigger, simulation and event selection

The events are selected by the HLT requiring an isolated lepton (electron or muon) with p_T of at least 15 GeV in combination with an online reconstructed H_T of at least 350 GeV. The HLT

is seeded by a Level 1 trigger satisfying $H_T^{L1} > 150\,\text{GeV}$. The trigger efficiency of $94 \pm 1\%$ is constant in the kinematic regime of the analysis, defined by lepton $p_T > 25\,\text{GeV}$ and $H_T > 500\,\text{GeV}$.

While the main backgrounds are determined from data as described in Section 5, simulated event samples are used to validate the techniques used, and to estimate extrapolation factors as needed. In addition, some subdominant backgrounds are estimated entirely from simulation. The MADGRAPH5 [21] event generator with the NNPDF3.0LO [22] parton distribution functions (PDF) is used for the simulation of $t\bar{t}$, W + jets, Z+jets, and QCD multijet events. Single-top events in the t and tW channels are generated using the POWHEGV1.0 [23–27] program, and in the s channel using MADGRAPH5_aMC@NLO [28], both with the NNPDF3.0NLO [22] PDF. All signal events are generated with MADGRAPH5, with up to two partons in addition to the gluino pair. The gluino decays are based on a pure phase-space matrix element [29]. The signal production cross sections [30–34] are computed at next-to-leading order (NLO) plus next-to-leading-logarithm (NLL) accuracy.

Parton showering and hadronization of all simulated samples use PYTHIA 8.2 [29]. Pileup is generated with a nominal distribution of proton-proton interactions per bunch crossing which is weighted to match the corresponding distribution in data. The detector response for all backgrounds is modelled using the GEANT4 [35] package, while for the signal the CMS fast simulation program [36, 37] is used to reduce computation time.

In order to separate possible new-physics signals from background, the L_T variable ist used, which is defined as the scalar sum of the lepton p_T and the missing transverse energy E_T^{miss}, reflecting the "leptonic" scale of the event. A minimum L_T of 250 GeV is required. With this requirement, the analysis is not only sensitive to events with high E_T^{miss}, but also to signal events with very low E_T^{miss}, but higher lepton p_T. An additional kinematic quantity important for the search is given by the "hadronic" scale of the event H_T, which is the scalar sum of the p_T of all selected jets in the event. For the requirement of $H_T > 500\,\text{GeV}$ the trigger is fully efficient. In addition to the minimum requirements on L_T and H_T, several search regions are defined in bins of $n_{\text{b-tag}}$, n_{jet}, L_T, and H_T.

Depending on the b-jet multiplicity, the analysis is sensitive to different models. Defining search bins in b-jet multiplicity enables the analysis to target specific event topologies and to separate them from standard model (SM) backgrounds. The phase space is separated into exclusive [0, 1, 2, $\geq$ 3] b-tagged jet categories when defining search bins, with a minimum b-jet p_T of 30 GeV. For the simplified model T1t^4, we expect a large number of jets and find that the n-jet distribution peaks at 8 or more jets. We require at least six jets for the multi-b analysis and define two independent n_{jet} categories of 6-8 and $\geq$ 9. The zero-b analysis, where the investigated simplified model (T5q^{4}WW) has fewer jets, requires in the signal region 5, 6-7, or $\geq$ 8 jets. Some SUSY models imply very high hadronic event activity. To accommodate this, we define search bins in H_T: $500 < H_T < 750\,\text{GeV}$, $750 < H_T < 1250\,\text{GeV}$, and $H_T > 1250\,\text{GeV}$. Figure 2 shows the H_T distribution for the multi-b analysis and the L_T distribution for the 0-b selection.

After this preselection, the main backgrounds are leptonically decaying W + jets and semi-leptonic $t\bar{t}$ events. For these backgrounds which both contain one lepton and one neutrino in the final state, the azimuthal angle between the W-boson candidate and the charged lepton, $\Delta\Phi$, is expected to be small, while the signal has an almost uniform distribution. Therefore, the region with large $\Delta\Phi$ is defined as the signal region, while the events with small $\Delta\Phi$ are used as the control sample. The ratio of control to signal region is determined in a side band with a lower number of jets, as described in Section 5. For the zero-b analysis, $\Delta\Phi$ is required to be larger than 1.0 for most regions except for high L_T regions, where the requirement is relaxed to

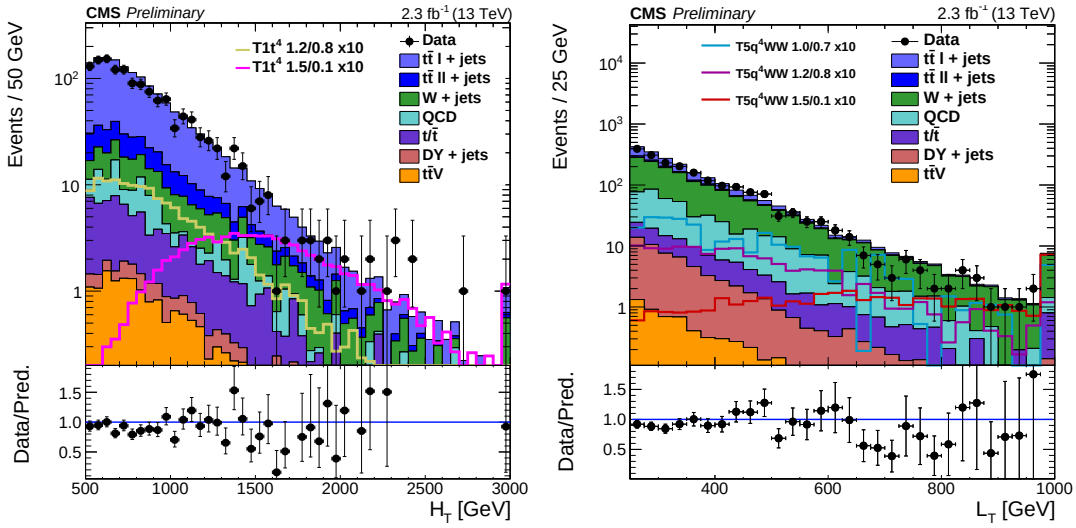

(a) (b)

Figure 2: The H_T distribution for the multi-b analysis in (left) and the L_T distribution for the zero-b analysis (right), both after the preselection, requiring at least six jets for the multi-b analysis, of which at least one is b-tagged, and at least five jets for the zero-b analysis, with no b-tagged jet. A minimum H_T of 500 GeV and a minimum L_T of 250 GeV is required in addition to exactly one lepton with $p_T > 25$ GeV. The simulated background events are stacked on top of each other, and several signal points are overlaid for illustration without being stacked. For the multi-b analysis, the model T1t^4 1.2/0.8 (T1t^4 1.5/0.1) corresponds to a gluino mass of 1.2 TeV (1.5 TeV) and neutralino mass of 0.8 TeV (0.1 TeV), respectively. For the zero-b analysis, the model T5q^{4}WW 1.0/0.7 (T5q^{4}WW 1.2/0.8 and T5q^{4}WW 1.5/0.1) corresponds to a gluino mass of 1.0 TeV (1.2 TeV and 1.5 TeV) and neutralino mass of 0.7 TeV (0.8 TeV and 0.1 TeV), respectively. For the latter, the intermediate chargino mass is fixed at 0.85 TeV (1.0 TeV and 0.8 TeV).

0.75, while the multi-b analysis has a relaxed $\Delta\Phi$ requirement of 0.75 and 0.5 for medium and high L_T regions. The $\Delta\Phi$ distribution is shown in Fig. 3 after the preselection for the zero-b and for the multi-b analysis.

A strong separation power in single-lepton searches is associated with L_T. Therefore, the search bins are defined as $250 < L_T < 350$ GeV, $300 < L_T < 450$ GeV, $450 < L_T < 600$ GeV, and $L_T > 600$ GeV. The search bins are defined such that high enough statistics is available in all bins to predict the background in the signal region. The bin boundaries in H_T and L_T are aligned for both zero- and multi-b analyses. The definitions of all signal regions are given in Table 1.

5 Background estimation

The dominant backgrounds in this analysis are $\mathrm{t\bar{t}}$ and W + jets events with relative yields depending on the multiplicity of b-tagged jets and the kinematic region. To determine these backgrounds, we define for each bin in L_T, H_T, and $n_{\text{b-tag}}$ two regions: the signal region (SR) with large values of $\Delta\Phi$, and the control region (CR) with low values of $\Delta\Phi$, with the explicit separation requirement depending on the L_T value as shown in Table 1. In addition, we define side band (SB) and main band (MB) regions, which have equal L_T and H_T requirements, but a different number of jets, which is lower in the SB region. These SB regions are used to determine the ratio between control and signal region, R_{CS}, from data for each L_T, H_T, and $n_{\text{b-tag}}$ region

Table 1: Signal regions and the corresponding $\Delta\Phi$ requirement.

n_{jet}	$n_{\text{b-tag}}$	L_{T} [GeV]	H_{T} [GeV]	$\Delta\Phi$
[6,8]	$= 1, = 2, \geq 3$	$[250, 350]$	$[500, 750]$, ≥ 750	1.0
		$[350, 450]$	$[500, 750]$, ≥ 750	0.75
	$= 1, \geq 2$	$[450, 600]$	$[500, 1250]$, ≥ 1250	
		≥ 600	$[500, 1250]$, ≥ 1250	0.5
≥ 9	$= 1, = 2$	$[250, 350]$	$[500, 1250]$, ≥ 1250	1.0
	≥ 3		≥ 500	
	$= 1, = 2, \geq 3$	$[350, 450]$	≥ 500	0.75
	$= 1, \geq 2$	≥ 450	≥ 500	
5	0	$[250, 350]$, $[350, 450]$, ≥ 450	≥ 500	1.0
[6,7]		$[250, 350]$, $[350, 450]$	$[500, 750]$, ≥ 750	
		≥ 450	$[500, 1000]$, ≥ 1000	0.75
≥ 8		$[250, 350]$	$[500, 750]$, ≥ 750	1.0
		$[350, 450]$, ≥ 450	≥ 500	0.75

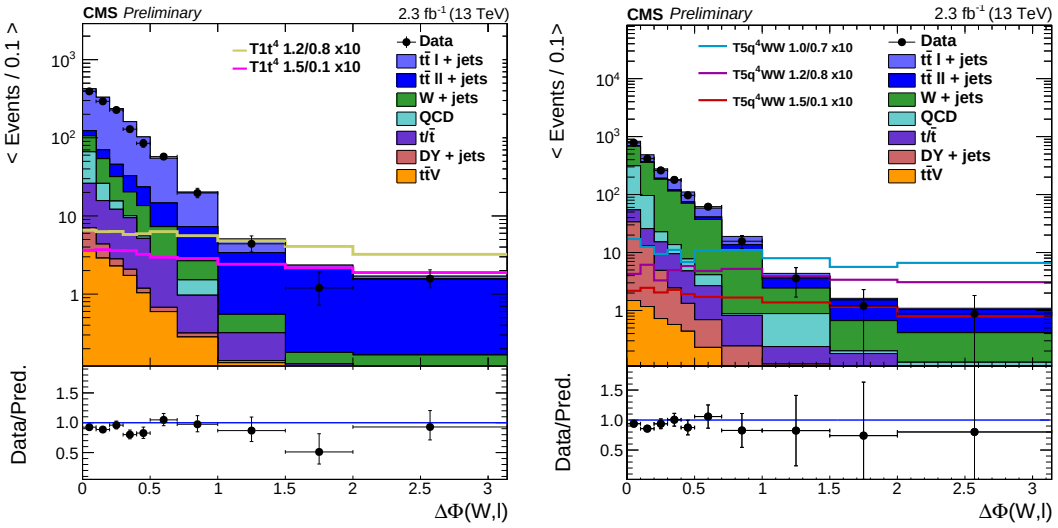

(a) (b)

Figure 3: Comparison of the $\Delta\Phi$ distribution for the multi-b (left) and zero-b analysis (right) after the preselection, requiring at least six jets for the multi-b analysis, of which at least one is b-tagged, and at least five jets for the zero-b analysis, with no b-tagged jet. A minimum H_{T} of 500 GeV and a minimum L_{T} of 250 GeV is required in addition to exactly one lepton with $p_{\text{T}} > 25$ GeV. The simulated background events are stacked on each other, and several signal points are overlayed without being stacked for illustration. For the multi-b analysis, the model T1t^4 1.2/0.8 (T1t^4 1.5/0.1) corresponds to a gluino mass of 1.2 TeV (1.5 TeV) and neutralino mass of 0.8 TeV (0.1 TeV), respectively. For the zero-b analysis, the model T5q^{4}WW 1.0/0.7 (T5q^{4}WW 1.2/0.8 and T5q^{4}WW 1.5/0.1) corresponds to a gluino mass of 1.0 TeV (1.2 TeV and 1.5 TeV) and neutralino mass of 0.7 TeV (0.8 TeV and 0.1 TeV), respectively. For the latter, the intermediate chargino mass is fixed at 0.85 TeV (1.0 TeV and 0.8 TeV).

separately. The background in each SR is then determined by the transfer factor R_{CS} multiplied

by the number of events in the corresponding CR. To account for possible differences in this extrapolation from SB to MB as a function of jet multiplicity, we define multiplicative correction factors κ from simulation.

When requiring one b-tag and four or five jets, about 80% $t\bar{t}$ events and 15%-20% W + jets and single top events are expected, while in all other multi-b regions, $t\bar{t}$ is completely dominant. Having only one physics background that dominates, a single R_{CS} factor is defined in the multi-b analysis for each L_T, H_T, and $n_{b\text{-tag}}$ range. When requiring zero b-tagged jets, both backgrounds, W + jets and $t\bar{t}$, are of equal importance. Here, an extension of the multi-b strategy is employed, which takes into account differences in the R_{CS} values for these two backgrounds.

The low $\Delta\Phi$ control regions include 10-15% QCD background that is subtracted before extrapolating from CR to SR because no such background exists in the SR. The transfer factor is determined in data in the SB region with a lower number of jets, for each signal bin separately:

$$R_{CS}^{data} = \frac{N_{data}^{SR}}{N_{data}^{CR} - N_{QCD\ estimate}^{CR}} \quad . \tag{1}$$

An overview of all regions used in this analysis is given in Table 2.

Table 2: Overview of the definitions of sideband and mainband regions.

Analysis	Multi-b analysis		Zero-b analysis	
$n_{b\text{-tag}}$	$n_{b\text{-tag}} = 0$	$n_{b\text{-tag}} \geq 1$	$n_{b\text{-tag}} = 0$	$n_{b\text{-tag}} = 1$
$n_{jet} = 3$	QCD Fit (el. sample)		$R_{CS}(W^{\pm})$ det. (μ sample), QCD Fit (el. sample)	
$n_{jet} = 4$		R_{CS} det.		$R_{CS}(t\bar{t})$ det.
$n_{jet} = 5$			MB	
$n_{jet} \geq 6$		MB		

5.1 R_{CS} method for $n_{b\text{-tag}} \geq 1$

For the multi-b analysis the SB region, where R_{CS} is determined, is required to have four or five jets, while the the MB region satisfies $n_{jet} \in [6-8]$ or $n_{jet} \geq 9$. For brevity, both of these MB jet multiplicity regions will be referred to as n_{jet}^{SR} in the following formulae. The expected number of background events in the SR, MB is then given by:

$$N_{MB}^{SR}(n_{b\text{-tag}}) = R_{CS}^{data}(n_{b\text{-tag}},\ n_{jet} \in [4,5]) \cdot \kappa_{EWK} \cdot \left[N_{data}^{CR}(n_{b\text{-tag}},\ n_{jet}^{SR}) - N_{QCD\ estimate}^{CR} \right] \quad , \text{ with} \tag{2}$$

$$\kappa_{EWK} = \frac{R_{CS}^{MC}(n_{b\text{-tag}},\ n_{jet}^{SR},\ EWK)}{R_{CS}^{MC}(n_{b\text{-tag}},\ n_{jet} \in [4,5],\ EWK)} \quad , \tag{3}$$

where R_{CS}^{data} is the transfer factor determined from data in the SB region with a lower number of jets, and N_{data}^{CR} the number of counted data events in the CR of the MB region. When referring to backgrounds other than QCD, the label EWK will be used. The residual difference between the R_{CS} in the SB and MB is evaluated in simulation as a correction factor κ_{EWK} given

in Equation 3, where $R_{CS}^{MC}(n_{b\text{-tag}},\ n_{jet}^{SR})$ is the R_{CS} in a signal MB region from simulation and $R_{CS}^{MC}(n_{b\text{-tag}},\ n_{jet} \in [4,5])$ is the simulated R_{CS} in the corresponding SB region.

The κ_{EWK} factor is determined for each search bin separately, except that an overall κ_{EWK}-factor is applied for the $n_{b\text{-jet}} \geq 2$ search bins with the same H_T and L_T, taking advantage of the fact that the κ_{EWK} factors are very similar for the different number of b-tags. Similarly, R_{CS} at very high H_T is determined jointly across all three $n_{b\text{-tag}}$ bins to increase statistics, as the overall uncertainty of the background prediction for several of the search bins is dominated by the statistical uncertainty due to the low number of events in the CR of the main band.

As the prediction extends from $n_{jet} \in [4,5]$ to two search bins with $n_{jet} \in [6-8]$ and $n_{jet} \geq 9$, it is important to understand the origin of all differences in detail. Two important aspects play a role when R_{CS} is compared between SB and MB: the relative fraction of a certain background, and the corresponding R_{CS} value of this component. For semileptonic $t\bar{t}$ events, R_{CS} typically has values of 0.01 to 0.02, depending on the search bin. Similar values, ranging from 0.01 to 0.04 are found for W + jets events. In events with more than one high p_T neutrino, e.g. in $t\bar{t}$ events in which both W bosons decay leptonically, R_{CS} is higher with values of around 0.5. This is expected from Fig. 3 which shows that in the $\Delta\Phi$ tail a large fraction of events is due to dileptonic $t\bar{t}$, while the low-$\Delta\Phi$ region is dominated by events with only one neutrino. A larger R_{CS} is also expected for events with three neutrinos, such as $t\bar{t}Z$, when the $t\bar{t}$ system decays semileptonically and the Z boson decays to two neutrinos. Thus it is important that the background composition does not change very much with increasing jet multiplicity when going from SB to MB for backgrounds with very different values of R_{CS}.

Most of the signal bins with 6 or more jets are dominated by semileptonic $t\bar{t}$ events, therefore this background dominates the total R_{CS} value of ~ 0.05. As the R_{CS} for dileptonic $t\bar{t}$ events is an order of magnitude larger than for semileptonic $t\bar{t}$ events, a slight change in composition in the CR when going from low to high n_{jet} multiplicity translates into a κ_{EWK} slightly different from one. This change in the amount of dileptonic $t\bar{t}$ is accounted for by assigning an uncertainty on the n_{jet} extrapolation based on a dileptonic control sample in data.

5.2 R_{CS} method for $n_{b\text{-tag}} = 0$

For search bins where b-tagged jets are vetoed, the background contributions from W + jets and $t\bar{t}$ events are estimated by applying the R_{CS} method separately to each of the two components. This strategy implies the use of two sidebands enriched in W + jets and $t\bar{t}$ events, respectively. For each L_T and H_T bin we denote the n_{jet} signal region by n_{jet}^{SR} and write the total background in this SR (with a $\Delta\Phi$ requirement as shown in Table 1) as:

$$N_{MB}^{SR}(0b) \quad = \quad N_{W}^{SR}(0b) + N_{t\bar{t}}^{SR}(0b) + N_{other}^{SR(MC)}(0b) \tag{4}$$

where the number of predicted W + jets and $t\bar{t}$ events is denoted by N_W^{SR} and $N_{t\bar{t}}^{SR}$, respectively. Additional backgrounds from rare sources are estimated from simulation and denoted by $N_{other}^{SR(MC)}$.

The expected number of events for each of the components can be described by:

$$N_i^{SR} = N_{data}^{CR} \cdot f_i \cdot R_{CS}^i \text{ , with } i = [W, t\bar{t}] \tag{5}$$

where N_{CR}^{data} is the total number of events in the CR of the mainband and f_i is the relative yield of component i. The relative contributions of the two components are determined by a fit of templates obtained from simulation to the $n_{b\text{-jet}}$ multiplicity distribution in the CR of the

MB region. The contribution of the QCD multijet background in the CR is fixed to the yield estimated from data as described in Section 5.3. The contribution of other, rare background components is obtained from simulation here as well, as is done in the SR. Uncertainties in these two components are propagated as systematic uncertainties to the final prediction. Examples of these fits are shown in Fig. 4.

Two R_{CS} values for W + jets and $\mathrm{t\bar{t}}$ are measured in two low n_{jet} SB regions. For the $\mathrm{t\bar{t}}$ estimate a sideband with the requirements $4 \leq n_{\mathrm{jet}} \leq 5$ and $n_{\text{b-tag}} = 1$ is used. The $R_{\mathrm{CS}}^{\mathrm{t\bar{t}}}$ is then given by:

$$R_{\mathrm{CS}}^{\mathrm{t\bar{t}}}(0\mathrm{b}, n_{\mathrm{jet}}^{\mathrm{SR}}) = \kappa_{\mathrm{b}} \cdot \kappa_{\mathrm{t\bar{t}}} \cdot R_{\mathrm{CS}}^{\mathrm{data}}(1\mathrm{b},\ n_{\mathrm{jet}} \in [4,5]) \quad . \tag{6}$$

The correction factor κ_{b} corrects for a potential difference of $R_{\mathrm{CS}}^{\mathrm{t\bar{t}}}$ between samples with 0 or 1 b jet and for the small contributions of backgrounds other than $\mathrm{t\bar{t}}$ or QCD multijet events. The factor $\kappa_{\mathrm{t\bar{t}}}$ corrects for a residual dependence of $R_{\mathrm{CS}}^{\mathrm{t\bar{t}}}$ on n_{jet}, in analogy to the κ_{EWK} factor defined in Section 5.1. Both values, κ_{b} and $\kappa_{\mathrm{t\bar{t}}}$, are close to unity, and statistical uncertainties from the simulation are propagated to the predicted yields.

Similarly, the W + jets contribution is estimated using R_{CS} values from a sideband with $3 \leq n_{\mathrm{jet}} \leq 4$ and $n_{\text{b-jet}} = 0$. With respect to the SB used for the estimate of $R_{\mathrm{CS}}^{\mathrm{t\bar{t}}}$ a lower jet multiplicity is chosen in order to limit the contamination from $\mathrm{t\bar{t}}$ events. Only the muon channel is used since it has a negligible contamination from QCD multijet events, contrary to the electron channel. A systematic uncertainty is derived from simulation in order to cover potential differences between the μ and the combined e and μ samples. The $R_{\mathrm{CS}}^{\mathrm{W}}$ is given by:

$$R_{\mathrm{CS}}^{\mathrm{W}}(0\mathrm{b},\ n_{\mathrm{jet}}^{\mathrm{SR}}) = \kappa_{\mathrm{W}} \cdot R_{\mathrm{CS}}^{\mathrm{data(corr)}}(0\mathrm{b},\ n_{\mathrm{jet}} \in [3,4]) \quad . \tag{7}$$

Again, the factor κ_{W} corrects for a residual dependence of $R_{\mathrm{CS}}^{\mathrm{W}}$ on the jet multiplicity,. The raw value of $R_{\mathrm{CS}}^{\mathrm{data}}$ measured in the SB has to be corrected for the contamination of $\mathrm{t\bar{t}}$ events. The $\mathrm{t\bar{t}}$ yields are subtracted in the numerator and denominator according to:

$$R_{\mathrm{CS}}^{\mathrm{data(corr)}}(0\mathrm{b}, n_{\mathrm{jet}} \in [3,4]) = \frac{N_{\mathrm{data}}^{SR} - R_{\mathrm{CS}}^{\mathrm{t\bar{t},MC}} \cdot f_{\mathrm{t\bar{t}}} \cdot N_{\mathrm{data}}^{\mathrm{CR}}}{(1 - f_{\mathrm{t\bar{t}}}) \cdot N_{\mathrm{data}}^{\mathrm{CR}}} \quad . \tag{8}$$

The event yields N_{data}^{CR} and N_{data}^{SR} are measured in the control and signal regions of the sideband. The fraction of $\mathrm{t\bar{t}}$ events $f_{\mathrm{t\bar{t}}}$ is again obtained by a fit to the $n_{\text{b-jet}}$ multiplicity in the CR of the SB. The R_{CS} value for $\mathrm{t\bar{t}}$ in this SB is obtained from simulation.

Systematic uncertainties are assigned to $\kappa_{\mathrm{t\bar{t}}}$ and κ_{W} according to the difference between the R_{CS} values in the sideband and the result of a linear fit over the full range of n_{jet}.

5.3 QCD background estimation

QCD multijet events enter this analysis mostly when reconstructed electrons originate from misidentified jets or from photon conversion in the inner detector. This background is estimated from the amount of 'anti-selected' electron candidates in each region, where anti-selected electrons have to pass looser identification and isolation requirements but fail the criteria of the medium electron working point. These events are scaled by the ratio of 'fake' QCD electrons passing the tight electron identification requirements to the number of anti-selected electrons, which is determined from a QCD-enriched control sample with zero b-tagged jets

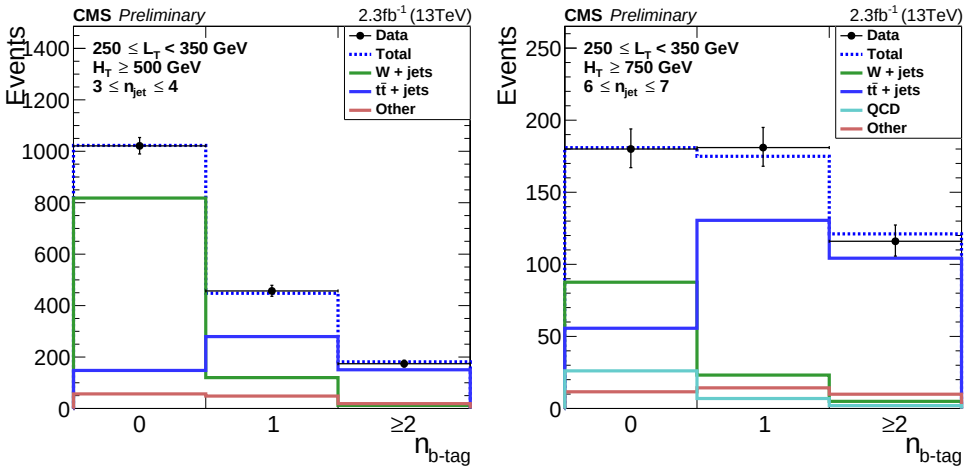

(a) $3 \leq n_{\text{jet}} \leq 4$ (b) $6 \leq n_{\text{jet}} \leq 7$

Figure 4: Fits to the $n_{\text{b-tag}}$ multiplicity for control regions in (a) $3 \leq n_{\text{jet}} \leq 4$ ($250 \leq L_{\text{T}} < 350\,\text{GeV}$, $H_{\text{T}} \geq 500\,\text{GeV}$, $\Delta\Phi < 1$, muon channel) and (b) $6 \leq n_{\text{jet}} \leq 7$ ($250 \leq L_{\text{T}} < 350\,\text{GeV}$, $H_{\text{T}} \geq 750\,\text{GeV}$, $\Delta\Phi < 1$) in data. The solid lines represent the templates scaled according to the fit result (blue for $\text{t}\bar{\text{t}}$, green for W + jets, turquoise for QCD and red for the remaining backgrounds), the dashed line shows the sum after fit, and the markers represent data.

and three or four jets. The estimation method has been introduced earlier [1, 38], and relies on the L_{P} variable:

$$L_{\text{P}} = \frac{p_{\text{T}}(l)}{p_{\text{T}}(W)} \cos(\Delta\Phi) \quad , \tag{9}$$

which reflects the effective lepton polarization from the W decay. Its shape, a falling distribution between 0 and 1, is well known for SM backgrounds like $\text{t}\bar{\text{t}}$ and W + jets, while QCD multijet events have a different shape, with a peak at $L_{\text{P}} \approx 1$.

The ratio of selected to anti-selected electrons is obtained from a fit to the L_{P} distribution in bins of L_{T}. The shape of the QCD multijet contribution used in the fit is taken from the anti-selected sample, while the shape of all other contributions is taken from simulation, as its behavior due to the W polarization is well understood. The ratios are found to be in the range 0.1–0.2.

In principle, the R_{CS} method requires the knowledge of the QCD contribution in the signal and control regions separately. Since the QCD background estimation is performed inclusively with respect to $\Delta\Phi$, an R_{CS} factor for QCD multijet events is determined as well. In practice, the resulting R_{CS} values are all found to be below 2%, the QCD contamination is thus negligible for the SR. Therefore, the previously described R_{CS} method takes into account only the QCD contribution in the CR, as written in Eq. 1. For the muon channel the expected contribution from QCD multijet background is expected to be much smaller. In order to estimate this contribution, a similar procedure to the one outlined above is applied and a 100% uncertainty is assigned.

6 Systematic uncertainties

Systematic uncertainties affect this analysis either by influencing κ, and thus the background prediction, or by affecting the expected signal yield.

The main systematic uncertainty of this analysis is due to the extrapolation of R_{CS} from the SB with a lower number of jets to the MB with a higher number of jets. Here, the ratio of the semileptonic to dileptonic $t\bar{t}$ decays for different number of reconstructed jets is of major importance, since the total R_{CS} is driven by the fraction of the two decays and their corresponding R_{CS} value, which differs significantly for semileptonic and dileptonic $t\bar{t}$ events. To ensure that the data are described well by simulation, a high-purity dilepton $t\bar{t}$ control sample is selected by requiring two opposite-sign leptons. For same-flavor leptons it is additionally required that the invariant mass of the lepton pair is more than 10 GeV away from the Z boson mass peak. In order to mock up the feed-down of the dileptonic events into the single-lepton selection, one of the two leptons is deleted from the event. To crudely mimic a hadronic tau decay for this "lost lepton", a response of $\sim 2/3$ is assumed, counting it as an additional jet, and adding it to E_T^{miss} accordingly. As a consequence, L_T, $\Delta\Phi$, and H_T of the now "single-leptonic" event are recalculated. In order to maximize the number of events defining the control region, no $\Delta\Phi$ cut is applied and all events are used twice, with each reconstructed lepton being considered as lost lepton at a time. The jet multiplicity distribution after the single-lepton baseline selection (excluding the signal regions) and the dileptonic control region are then compared to the simulation. While observing in general the same behavior, the double ratio of the two ratios of data over simulation is used to determine the uncertainty on the simulation, which is mainly driven by the statistical error of the data samples.

Compared to the uncertainty due to the dileptonic control sample, all other uncertainties are smaller. Corrections to the jet energy scale (JEC) are varied within the given uncertainties as a function of jet p_T and η. These variations are also propagated to E_T^{miss}. The scale factors applied to the efficiencies for the identification of b-quark and for the misidentification of c-quark, light quark or gluon jets are scaled up and down according to their uncertainties. Uncertainties for the efficiency of lepton reconstruction and identification are derived in the same way. For pileup, a 5% uncertainty on the inelastic cross section is used to derive the impact of the uncertainty on the pileup profile. All of these uncertainties apply both to the background prediction and the signal yield. The luminosity is measured with the Pixel Cluster Counting method and the absolute luminosity scale calibration is derived from an analysis of Van der Meer Scans performed in August 2015, resulting in an uncertainty of 2.7% [39].

Both the W cross section and the $t\bar{t}$ cross section are varied by a conservative 30% in order to cover possible biases in the estimation of the background composition in terms of W + jets vs. $t\bar{t}$ events. These variations have a small impact on the zero-b analysis where the relative fraction of the two processes is determined in a fit. The polarization of W bosons in W+jets events is varied by 10% guided by theory uncertainty predictions and measurements found in [40–43]. For $t\bar{t}$ events, the polarization is varied only by 5%, i.e. events are reweighted by w= 1 +(0.1 or 0.05)*(1-cos(θ^*))^2, where cos(θ^*) is the angle between charged lepton and W boson in the W rest-frame. For W + jets this is done twice, once treating both charges the same and once only reweighting positive charges, and the bigger resulting uncertainty is chosen. For the $t\bar{t}$ background, the $t\bar{t}$ system is reweighted by a weight defined by $\sqrt{SF(t) \cdot SF(\bar{t})}$ with $SF = \exp(0.156 - 0.00137 \cdot p_T(t))$ or 0.5, if the weight is smaller than 0.5. The difference between the values of κ in the reweighted and the original sample is taken as the uncertainty. The $t\bar{t}V$ cross-section is conservatively varied by 100%. The systematic uncertainty on the QCD estimation depends on n_{jet} and $n_{b\text{-}tag}$, and ranges from 25% to 100%.

In addition, for the zero-b analysis a systematic uncertainty based on the result of linear fits of R_{CS} is applied as a function of n_{jet} as described in Section 5.2. For the zero-b analysis, 50% cross section uncertainty is applied to all backgrounds other than W + jets, $t\bar{t}$, $t\bar{t}V$, and QCD.

For the signal, an uncertainty on initial-state radiation (ISR) is applied, based on the p_T of the gluino-gluino system, which amounts to 15% uncertainty for gluino-gluino p_T between 400 and 600 GeV, and 30% for higher momentum. Uncertainty on the signal cross section are taken into account as well.

The impact of the systematic uncertainties on the total background prediction for the multi-b and zero-b analysis are summarized in Table 3. While the systematic uncertainty is determined for each signal point, the uncertainties typical for most signals are summarized for illustration in Table 4.

Table 3: Summary of the systematic uncertainties for the total background prediction for the multi-b and for the zero-b analysis.

Source	Uncertainty [%] for multi-b	Uncertainty [%] for zero-b
dilepton control sample	8-20	8-40
JEC	0.2-11	0.6-8.2
b-tagging	0.1-17	1.4-4.5
$\sigma(W + \text{jets})$	0.3-6.4	<2.5
W polarization variation	0.1-2	0.2-3.4
$\sigma(t\bar{t}V)$	0.1-5	0.2-2.9
top p_T reweighting	0.1-10	0.1-7.1
pileup	0.3-23	0.1-10
R_{CS} fit	–	3.3-35
Total	8.0-28	10-54
MC statistics	3-30	8-48

Table 4: Summary of the systematic uncertainties and their average effect on the example signal points. The values are very similar for the multi-b and the zero-b analysis, and are mostly larger for compressed scenarios, where the mass difference between gluino and neutralino is small.

Source	Uncertainty [%]
Trigger	1
PU	5
Lepton efficiency	5
Luminosity	2.7
ISR	3-20
b-tag HF	6-10
b-tag LF	2-3
JEC	3-10
Factorization/renormalization scale	< 3
Total	12-26

7 Results and interpretation

The backgrounds for all search regions are determined as described previously in different side band regions with lower jet or b-jet multiplicities. The multi-b analysis consists of 30 exclusive bins, while for the zero-b analysis contains 13 exclusive categories, as introduced in previous

chapters. The result of the background prediction (in red), the observed data (black), and the expected number of background events from simulation are shown in Figure 5 for the multi-b case and in Figure 6 the zero-b case.

Table 5: Summary of the results in the multi-b search.

n_{jet}	L_T [GeV]	H_T [GeV]	$n_{\text{b-jet}}$	Bin name	Expected signal T1t^4 $m_{\tilde{g}}/m_{\tilde{\chi}^0}$ [TeV] 1.5/0.1	1.2/0.8	Predicted background	Observed
[6, 8]	[250, 350]	[500, 750]	= 1	LT1, HT0, NB1	0.00 ± 0.00	0.41 ± 0.02	9.03 ± 2.07	9
			= 2	LT1, HT0, NB2	0.00 ± 0.00	0.67 ± 0.03	8.38 ± 2.10	2
			≥ 3	LT1, HT0, NB3i	0.00 ± 0.00	0.67 ± 0.03	1.23 ± 0.39	1
		≥ 750	= 1	LT1, HT1i, NB1	0.03 ± 0.00	0.15 ± 0.01	9.77 ± 2.99	14
			= 2	LT1, HT1i, NB2	0.07 ± 0.00	0.27 ± 0.02	7.08 ± 2.74	6
			≥ 3	LT1, HT1i, NB3i	0.07 ± 0.00	0.22 ± 0.02	0.85 ± 0.40	1
	[350, 450]	[500, 750]	= 1	LT2, HT0, NB1	0.00 ± 0.00	0.19 ± 0.02	2.42 ± 0.96	4
			= 2	LT2, HT0, NB2	0.01 ± 0.00	0.28 ± 0.02	0.89 ± 0.56	2
			≥ 3	LT2, HT0, NB3i	0.01 ± 0.00	0.24 ± 0.02	0.10 ± 0.08	0
		≥ 750	= 1	LT2, HT1i, NB1	0.08 ± 0.00	0.16 ± 0.01	3.61 ± 1.75	5
			= 2	LT2, HT1i, NB2	0.12 ± 0.01	0.24 ± 0.02	3.75 ± 1.90	2
			≥ 3	LT2, HT1i, NB3i	0.13 ± 0.01	0.19 ± 0.01	0.54 ± 0.35	0
	[450, 600]	[500, 1250]	= 1	LT3, HT01, NB1	0.07 ± 0.00	0.18 ± 0.02	4.11 ± 1.59	1
			≥ 2	LT3, HT01, NB2i	0.19 ± 0.01	0.42 ± 0.02	4.02 ± 2.11	0
		≥ 1250	= 1	LT3, HT2i, NB1	0.08 ± 0.00	0.02 ± 0.00	0.62 ± 0.69	1
			≥ 2	LT3, HT2i, NB2i	0.29 ± 0.01	0.08 ± 0.01	0.59 ± 0.66	1
	≥ 600	[500, 1250]	= 1	LT4i, HT01, NB1	0.18 ± 0.01	0.05 ± 0.01	0.60 ± 0.51	0
			≥ 2	LT4i, HT01, NB2i	0.57 ± 0.01	0.16 ± 0.01	0.25 ± 0.39	0
		≥ 1250	= 1	LT4i, HT2i, NB1	0.26 ± 0.01	0.07 ± 0.01	0.20 ± 0.27	0
			≥ 2	LT4i, HT2i, NB2i	0.95 ± 0.02	0.16 ± 0.01	0.42 ± 0.53	0
≥ 9	[250, 350]	[500, 1250]	= 1	LT1, HT01, NB1	0.01 ± 0.00	0.22 ± 0.02	0.52 ± 0.19	0
			= 2	LT1, HT01, NB2	0.01 ± 0.00	0.55 ± 0.03	0.23 ± 0.14	0
		≥ 500	≥ 3	LT1, HT0i, NB3i	0.08 ± 0.00	0.74 ± 0.03	0.32 ± 0.16	0
		≥ 1250	= 1	LT1, HT2i, NB1	0.02 ± 0.00	0.02 ± 0.01	0.17 ± 0.16	0
			= 2	LT1, HT2i, NB2	0.04 ± 0.00	0.05 ± 0.01	0.24 ± 0.31	0
	[350, 450]	≥ 500	= 1	LT2, HT0i, NB1	0.04 ± 0.00	0.23 ± 0.02	0.28 ± 0.14	0
			= 2	LT2, HT0i, NB2	0.10 ± 0.01	0.41 ± 0.02	0.05 ± 0.06	1
			≥ 3	LT2, HT0i, NB3i	0.12 ± 0.01	0.51 ± 0.02	0.04 ± 0.05	0
	≥ 450	≥ 500	= 1	LT3i, HT0i, NB1	0.29 ± 0.01	0.23 ± 0.02	0.31 ± 0.20	0
			≥ 2	LT3i, HT0i, NB2i	1.42 ± 0.02	0.99 ± 0.03	0.15 ± 0.13	0

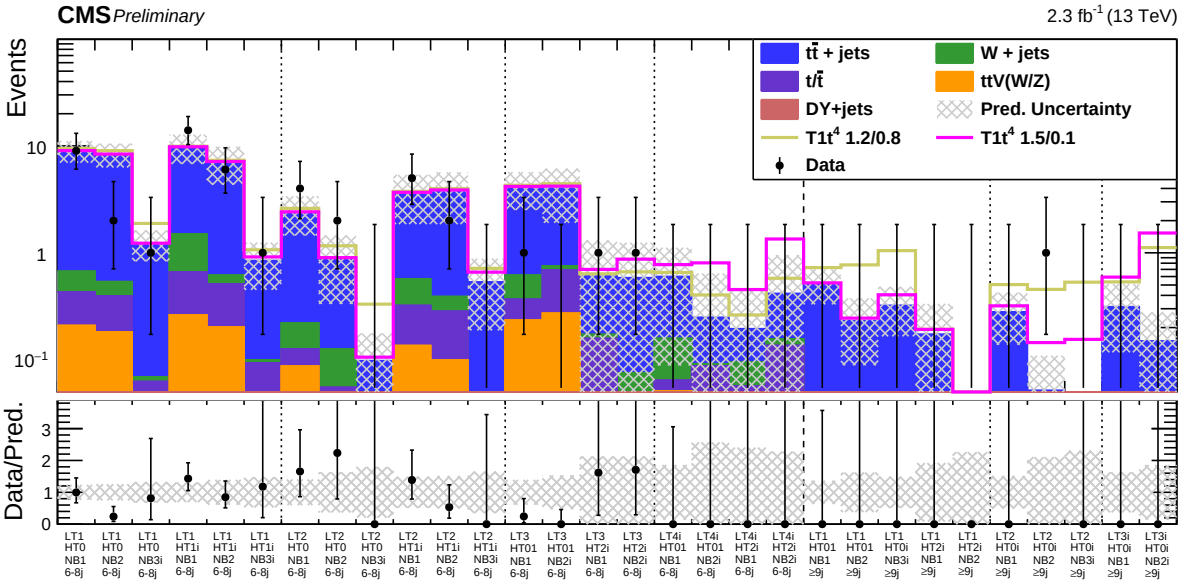

Figure 5: Multi-b analysis: The data-driven prediction is represented by the filled histograms preserving the individual background contributions from MC; the observed number of events is shown in black. The colored lines show two signal benchmark points stacked on the prediction.

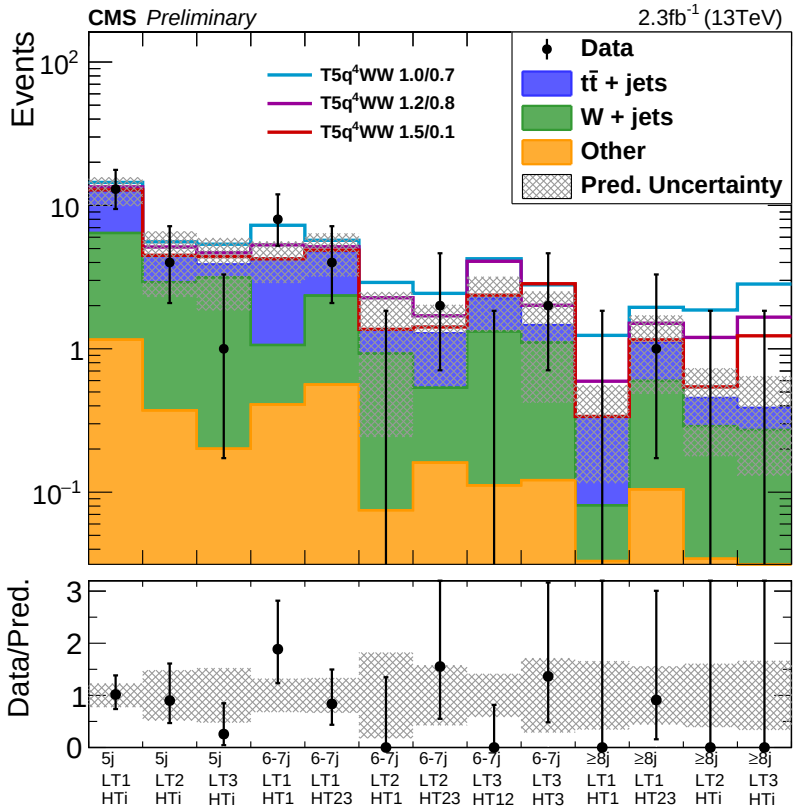

Figure 6: Zero-b analysis: observed and predicted event counts in the 13 signal regions. The black points show the number of observed events. The filled, stacked histograms represent the predictions for $t\bar{t}$, W + jets events, and the remaining backgrounds. The colored lines illustrate the expectations for three benchmark points of the T5q^{4}WW model. The lower panel shows the ratio between data and prediction. The error bars indicate the total statistical and systematic uncertainty on the ratio.

Table 6: Summary of the results of the zero-b search with 2.3 fb^{-1}.

n_{jet}	L_T [GeV]	H_T [GeV]	Bin name	Expected signal T5q^{4}WW $m_{\tilde{g}}/m_{\tilde{\chi}^0}$ [TeV] 1.0/0.7	1.2/0.8	1.5/0.1	Predicted background	Observed
5	[250, 350]	$\geq$ 500	LT1, HTi	1.67 ± 0.27	0.68 ± 0.07	0.03 ± 0.01	12.8 ± 2.91	13
	[350, 450]	$\geq$ 500	LT2, HTi	1.13 ± 0.22	0.68 ± 0.07	0.04 ± 0.01	4.45 ± 2.15	4
	$\geq$ 450	$\geq$ 500	LT3, HTi	1.48 ± 0.26	0.79 ± 0.08	0.51 ± 0.02	3.89 ± 2.03	1
[6,7]	[250, 350]	[500, 750]	LT1, HT1	3.03 ± 0.36	1.06 ± 0.09	0.0 ± 0.0	4.24 ± 1.37	8
		$\geq$ 750	LT1, HT23	0.92 ± 0.2	0.36 ± 0.05	0.08 ± 0.01	4.79 ± 1.6	4
	[350, 450]	[500, 750]	LT2, HT1	1.54 ± 0.26	0.9 ± 0.08	0.0 ± 0.0	1.37 ± 1.12	0
		$\geq$ 750	LT2, HT23	1.15 ± 0.21	0.41 ± 0.05	0.13 ± 0.01	1.29 ± 0.74	2
	$\geq$ 450	[500, 1000]	LT3, HT12	1.99 ± 0.29	1.83 ± 0.12	0.11 ± 0.01	2.25 ± 0.93	0
		$\geq$ 1000	LT3, HT3	1.33 ± 0.23	0.55 ± 0.06	1.38 ± 0.04	1.47 ± 1.04	2
$\geq$ 8	[250, 350]	[500, 750]	LT1, HT1	0.9 ± 0.2	0.26 ± 0.04	0.0 ± 0.0	0.34 ± 0.22	0
		$\geq$ 750	LT1, HT23	0.85 ± 0.19	0.41 ± 0.05	0.06 ± 0.01	1.1 ± 0.61	1
	[350, 450]	$\geq$ 500	LT2, HTi	1.41 ± 0.23	0.75 ± 0.07	0.09 ± 0.01	0.45 ± 0.28	0
	$\geq$ 450	$\geq$ 500	LT3, HTi	2.44 ± 0.31	1.27 ± 0.09	0.84 ± 0.03	0.39 ± 0.26	0

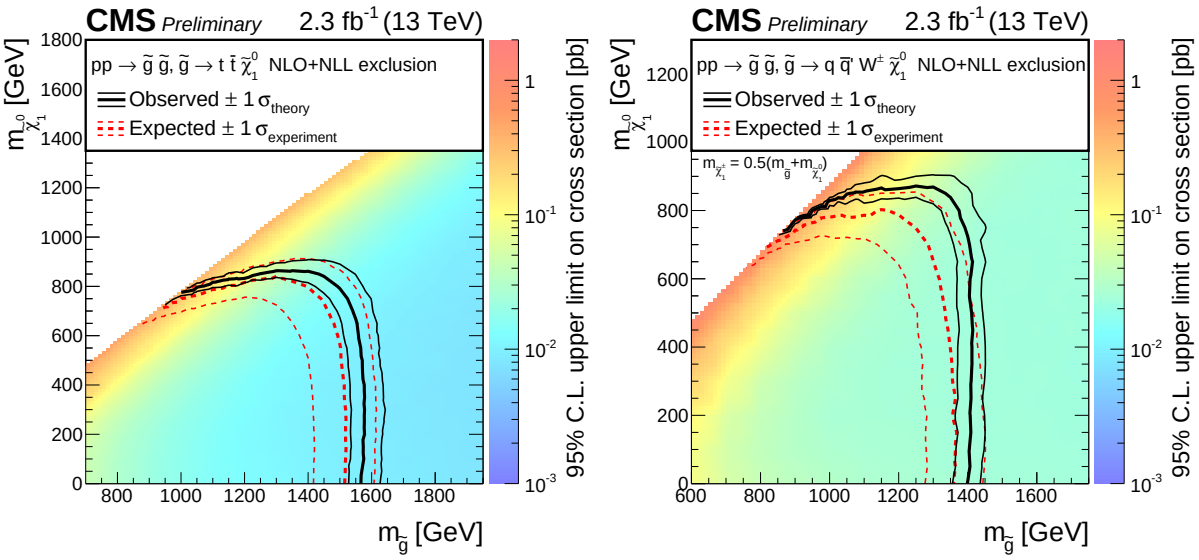

Figure 7: Cross section limits at 95% CL for the (left) T1t^4 and (right) T5q^{4}WW models as a function of the the gluino and LSP masses. In T5q^{4}WW, the pair-produced gluinos each decay to a quark-antiquark pair of the first or second generation ($q\bar{q}$), and a chargino ($\tilde{\chi}_1^{\pm}$) with its mass defined as $m_{\tilde{\chi}_1^{\pm}} = 0.5(m_{\tilde{g}} + m_{\tilde{\chi}_1^0})$. The black (red) lines correspond to the observed (expected) mass limits, with the solid lines representing the central values and the dashed lines the $\pm 1\sigma$ uncertainty bands related to the theoretical (experimental) uncertainties.

In order to set limits, a likelihood function is built that contains Poisson probability functions for all four data regions, needed to determine the background in the signal region of the main band. Additionally, the κ values derived from simulation are included to correct any residual differences between the side band and main band regions, and uncertainties on this value are incorporated with log-normal constraints. The estimated contribution from QCD multijet events in the two control regions is included as well. A profile likelihood ratio in the asymptotic approximation [44] is used as the test statistic. Limits are then calculated at the 95% confidence level using the CLs criterion [45, 46].

The cross section limits obtained for the T1t^4 model using the multi-b analysis, and for the T5q^{4}WW model using the zero-b analysis, are shown in Fig. 7 as a function of $m(\tilde{g})$ and $m(\tilde{\chi}_1^0)$, assuming branching ratio of 100% as shown in Fig. 1. Using the $\tilde{g}\tilde{g}$ pair production cross section calculated at next-to-leading order plus next-to-leading-logarithm accuracy, exclusion limits as a function of the $m_{\tilde{g}}/m_{\tilde{\chi}_1^0}$ mass hypothesis are set.

8 Summary

A search for supersymmetry has been performed with 2.3 fb^{-1} of pp collision data taken in 2015 with the CMS experiment. The data is analyzed in several exclusive categories, differing in the number of jets and b-tagged jets, the scalar sum of all jet transverse momenta and the scalar sum of the transverse missing momentum and the lepton. Background is rejected by requiring a large azimuthal angle between the lepton and the reconstructed W boson direction. No significant excess has been observed, and the results are interpreted in two simplified models describing gluino pair production. For a simplified model, where each gluino decays to a $t\bar{t}$ pair and the lightest neutralino, gluino masses up to 1.575 TeV can be excluded for neutralino

masses below 600 GeV. Neutralino masses below 850 GeV can be excluded for a gluino mass of 1.4 TeV. This extends the limits obtained from the 8 TeV searches by about 250 GeV. In a second simplified model gluino pair production is investigated as well, here with gluinos decaying to first or second generation squarks and a chargino, which then decays to a W boson and the lightest neutralino. The chargino mass in this decay chain is defined as $m_{\widetilde{\chi}_1^\pm} = 0.5(m_{\widetilde{g}} + m_{\widetilde{\chi}_1^0})$. In this model, gluino masses below 1.4 TeV are excluded for neutralino masses below 725 GeV.

A Cutflow

Table 7 contains the cutflow for the preselection. For the initial selection, one lepton and $H_T >$ 350 GeV is required.

Table 7: Yield table ($2.3\,\mathrm{fb}^{-1}$) for the baseline selection split for all backgrounds. The event yields in the last three lines are exclusive for the zero-b and the multi-b selection, respectively. The simulated events are corrected with scale factors to account for differences in the lepton identification and isolation efficiencies, as well as the b-tagging efficiency between simulation and data. The trigger efficiency is applied as well and a reweighting is applied to $\mathrm{t\bar{t}}$ events based on the p_T of the $\mathrm{t\bar{t}}$ system.

CUT	$\mathrm{T1t^4}1.2/0.8$	$\mathrm{T1t^4}1.5/0.1$	$\mathrm{T5q^4}1.2/1/0.8$	$\mathrm{T5q^4}1.5/0.8/0.1$	TT dilep.	TT rest	WJets	QCD	SingleT	DY	TTV	All BKG
one lepton and H_T >350 GeV	51	11	45.9	9.4	7757	70103	73488	28009	5284	6513	356	191513
no veto lepton	43	9.4	43.2	8.9	6471	68371	72986	27400	5144	5221	328	185922
$\mathrm{N}_{jet} \geq 5$	42	9.2	35.8	8.2	2868	41571	11453	5838	1388	1076	245	64441
$p_T^{j2} > 80\,\mathrm{GeV}$	37	9.2	33.9	8.2	2477	35572	10299	5102	1229	964	218	55862
$H_\mathrm{T} > 500\,\mathrm{GeV}$	30	9.2	27.4	8.2	1301	17655	6490	2377	711	575	143	29253
$L_\mathrm{T} > 250\,\mathrm{GeV}$	16	8.7	21.2	7.9	323	2380	1388	250	183	70	29	4623
$n_{\text{b-jet}} = 0$ and $\Delta\Phi > 0.75$	0.39	0.23	11.0	3.5	18	5.7	14	1.2	1.1	0.8	0.7	50
$n_{\text{b-jet}} \geq 1$, $n_{\text{jet}} \geq 6$	14	7.8	4.4	1.9	141	1111	122	30	60	6.8	15	1486
and $\Delta\Phi > 0.75$	9.4	5.3	2.9	1.2	52	38	4.8	0.2	3.7	0.2	2.1	102

References

[1] CMS Collaboration, "Search for supersymmetry in pp collisions at $\sqrt{s} = 7$ TeV in events with a single lepton, jets, and missing transverse momentum", *Eur.Phys.J.* **C73** (2013) 2404, doi:10.1140/epjc/s10052-013-2404-z, arXiv:1212.6428.

[2] CMS Collaboration, "Search for supersymmetry in final states with a single lepton, b-quark jets, and missing transverse energy in proton-proton collisions at $\sqrt{s} = 7$ TeV", *Phys.Rev.* **D87** (2013), no. 5, 052006, doi:10.1103/PhysRevD.87.052006, arXiv:1211.3143.

[3] ATLAS Collaboration, "Further search for supersymmetry at $\sqrt{s} = 7$ TeV in final states with jets, missing transverse momentum and isolated leptons with the ATLAS detector", *Phys. Rev.* **D86** (2012) 092002, doi:10.1103/PhysRevD.86.092002, arXiv:1208.4688.

[4] CMS Collaboration, "Search for supersymmetry in pp collisions at $\sqrt{s}$=8 TeV in events with a single lepton, large jet multiplicity, and multiple b jets", *Phys.Lett.* **B733** (2014) 328–353, doi:10.1016/j.physletb.2014.04.023, arXiv:1311.4937.

[5] ATLAS Collaboration, "Search for squarks and gluinos in events with isolated leptons, jets and missing transverse momentum at $\sqrt{s} = 8$ TeV with the ATLAS detector", *JHEP* **04** (2015) 116, doi:10.1007/JHEP04(2015)116, arXiv:1501.03555.

[6] ATLAS Collaboration, "Search for strong production of supersymmetric particles in final states with missing transverse momentum and at least three b-jets at $\sqrt{s}$= 8 TeV proton-proton collisions with the ATLAS detector", *JHEP* **10** (2014) 024, doi:10.1007/JHEP10(2014)024, arXiv:1407.0600.

[7] CMS Collaboration, "Search for supersymmetry in pp collisions at sqrt (s) = 13 TeV in the single-lepton final state using the sum of masses of large radius jets", CMS Physics Analysis Summary CMS-PAS-SUS-15-007, CERN, Geneva, 2015.

[8] ATLAS Collaboration, "Search for gluinos in events with an isolated lepton, jets and missing transverse momentum at $\sqrt{s} = 13$ TeV with the ATLAS detector", Conference Note ATLAS-CONF-2015-076, 2015.

[9] ATLAS Collaboration, "Search for pair-production of gluinos decaying via stop and sbottom in events with b-jets and large missing transverse momentum in $\sqrt{s} = 13$ TeV pp collisions with the ATLAS detector", Conference Note ATLAS-CONF-2015-067, 2015.

[10] CMS Collaboration, "The CMS experiment at the CERN LHC", *JINST* **3** (2008) S08004, doi:10.1088/1748-0221/3/08/S08004.

[11] CMS Collaboration, "Description and performance of track and primary-vertex reconstruction with the CMS tracker", *JINST* **9** (2014) P10009, doi:10.1088/1748-0221/9/10/P10009, arXiv:1405.6569.

[12] CMS Collaboration, "Performance of electron reconstruction and selection with the CMS detector in proton-proton collisions at $\sqrt{s} = 8$ TeV", *JINST* **10** (2015) P06005, doi:10.1088/1748-0221/10/06/P06005, arXiv:1502.02701.

[13] CMS Collaboration, "Performance of CMS muon reconstruction in pp collision events at $\sqrt{s} = 7$ TeV", *JINST* **7** (2012) P10002, doi:10.1088/1748-0221/7/10/P10002, arXiv:1206.4071.

[14] CMS Collaboration, "Particle-flow event reconstruction in CMS and performance for jets, taus, and $E_{\mathrm{T}}^{\mathrm{miss}}$", CMS Physics Analysis Summary CMS-PAS-PFT-09-001, CERN, 2009.

[15] CMS Collaboration, "Commissioning of the particle-flow event with the first LHC collisions recorded in the CMS detector", CMS Physics Analysis Summary CMS-PAS-PFT-10-001, CERN, 2010.

[16] CMS Collaboration, "Determination of jet energy calibration and transverse momentum resolution in CMS", *JINST* **6** (2011) P11002, doi:10.1088/1748-0221/6/11/P11002, arXiv:1107.4277.

[17] M. Cacciari and G. P. Salam, "Pileup subtraction using jet areas", *Phys. Lett. B* **659** (2008) 119, doi:10.1016/j.physletb.2007.09.077, arXiv:0707.1378.

[18] CMS Collaboration, "Identification of b-quark jets with the CMS experiment", *JINST* **8** (2013) P04013, doi:10.1088/1748-0221/8/04/P04013, arXiv:1211.4462.

[19] CMS Collaboration, "Identification of b quark jets at the CMS Experiment in the LHC Run 2", CMS Physics Analysis Summary CMS-PAS-BTV-15-001, CERN, 2016.

[20] CMS Collaboration, "Performance of b tagging at $\sqrt{s} = 8$ TeV in multijet, $\mathrm{t\bar{t}}$ and boosted topology events", CMS Physics Analysis Summary CMS-PAS-BTV-13-001, CERN, 2013.

[21] J. Alwall et al., "MadGraph5: going beyond", *JHEP* **06** (2011) 128, doi:10.1007/JHEP06(2011)128, arXiv:1106.0522.

[22] NNPDF Collaboration, "Parton distributions for the LHC Run II", *JHEP* **04** (2015) 040, doi:10.1007/JHEP04(2015)040, arXiv:1410.8849.

[23] P. Nason, "A New method for combining NLO QCD with shower Monte Carlo algorithms", *JHEP* **11** (2004) 040, doi:10.1088/1126-6708/2004/11/040, arXiv:hep-ph/0409146.

[24] S. Frixione, P. Nason, and C. Oleari, "Matching NLO QCD computations with Parton Shower simulations: the POWHEG method", *JHEP* **11** (2007) 070, doi:10.1088/1126-6708/2007/11/070, arXiv:0709.2092.

[25] S. Alioli, P. Nason, C. Oleari, and E. Re, "A general framework for implementing NLO calculations in shower Monte Carlo programs: the POWHEG BOX", *JHEP* **06** (2010) 043, doi:10.1007/JHEP06(2010)043, arXiv:1002.2581.

[26] S. Alioli, P. Nason, C. Oleari, and E. Re, "NLO single-top production matched with shower in POWHEG: s- and t-channel contributions", *JHEP* **09** (2009) 111, doi:10.1007/JHEP02(2010)011, 10.1088/1126-6708/2009/09/111, arXiv:0907.4076. [Erratum: JHEP02,011(2010)].

[27] E. Re, "Single-top Wt-channel production matched with parton showers using the POWHEG method", *Eur. Phys. J.* **C71** (2011) 1547, doi:10.1140/epjc/s10052-011-1547-z, arXiv:1009.2450.

[28] J. Alwall et al., "The automated computation of tree-level and next-to-leading order differential cross sections, and their matching to parton shower simulations", *JHEP* **07** (2014) 079, doi:10.1007/JHEP07(2014)079, arXiv:1405.0301.

[29] T. Sjöstrand et al., "An Introduction to PYTHIA 8.2", *Comput. Phys. Commun.* **191** (2015) 159–177, doi:10.1016/j.cpc.2015.01.024, arXiv:1410.3012.

[30] W. Beenakker, R. Höpker, M. Spira, and P. M. Zerwas, "Squark and gluino production at hadron colliders", *Nucl. Phys. B* **492** (1997) 51, doi:10.1016/S0550-3213(97)00084-9, arXiv:hep-ph/9610490.

[31] A. Kulesza and L. Motyka, "Threshold resummation for squark-antisquark and gluino-pair production at the LHC", *Phys. Rev. Lett.* **102** (2009) 111802, doi:10.1103/PhysRevLett.102.111802, arXiv:0807.2405.

[32] A. Kulesza and L. Motyka, "Soft gluon resummation for the production of gluino-gluino and squark-antisquark pairs at the LHC", *Phys. Rev. D* **80** (2009) 095004, doi:10.1103/PhysRevD.80.095004, arXiv:0905.4749.

[33] W. Beenakker et al., "Soft-gluon resummation for squark and gluino hadroproduction", *JHEP* **12** (2009) 041, doi:10.1088/1126-6708/2009/12/041, arXiv:0909.4418.

[34] W. Beenakker et al., "Squark and gluino hadroproduction", *Int. J. Mod. Phys. A* **26** (2011) 2637, doi:10.1142/S0217751X11053560, arXiv:1105.1110.

[35] S. Agostinelli et al., "GEANT4 — a simulation toolkit", *Nucl. Instr. and Meth. A* **506** (2003) 250, doi:10.1016/S0168-9002(03)01368-8.

[36] CMS Collaboration, "Fast simulation of the CMS detector", *J. Phys. Conf. Ser.* **219** (2010) 032053, doi:10.1088/1742-6596/219/3/032053. (D. Orbaker for the collaboration).

[37] CMS Collaboration, "Comparison of the fast simulation of CMS with the first LHC data", CMS Detector Performance Summary CMS-DP-2010-039, CERN, 2010.

[38] CMS Collaboration, "Measurement of the Polarization of W Bosons with Large Transverse Momenta in $W+$jets Events at the LHC", *Phys. Rev. Lett.* **107** (Jul, 2011) 021802, doi:10.1103/PhysRevLett.107.021802.

[39] CMS Collaboration, "CMS Luminosity Measurement for the 2015 Data Taking Period", CMS Physics Analysis Summary CMS-PAS-LUM-15-001, 2016.

[40] Z. Bern et al., "Left-Handed W Bosons at the LHC", *Phys. Rev.* **D84** (2011) 034008, arXiv:1103.5445.

[41] CMS Collaboration, "Angular coefficients of Z bosons produced in pp collisions at $\sqrt{s}$ = 8 TeV and decaying to $\mu^+\mu^-$ as a function of transverse momentum and rapidity", *Phys. Lett.* **B750** (2015) 154–175, doi:10.1016/j.physletb.2015.08.061, arXiv:1504.03512.

[42] CMS Collaboration, "Measurement of the Polarization of W Bosons with Large Transverse Momenta in W+Jets Events at the LHC", *Phys. Rev. Lett.* **107** (2011) 021802, doi:10.1103/PhysRevLett.107.021802, arXiv:1104.3829.

[43] ATLAS Collaboration, "Measurement of the polarisation of W bosons produced with large transverse momentum in pp collisions at $\sqrt{s} = 7$ TeV with the ATLAS experiment", *Eur. Phys. J.* **C72** (2012) 2001, doi:10.1140/epjc/s10052-012-2001-6, arXiv:1203.2165.

[44] G. Cowan, K. Cranmer, E. Gross, and O. Vitells, "Asymptotic formulae for likelihood-based tests of new physics", *Eur. Phys. J. C* **71** (2011) 1554, doi:10.1140/epjc/s10052-011-1554-0,10.1140/epjc/s10052-013-2501-z, arXiv:1007.1727. [Erratum: Eur. Phys. J.C73,2501(2013)].

[45] T. Junk, "Confidence level computation for combining searches with small statistics", *Nucl. Instr. and Meth. A* **434** (1999) 435, doi:10.1016/S0168-9002(99)00498-2, arXiv:hep-ex/9902006.

[46] A. L. Read, "Presentation of search results: the CL_s technique", *J. Phys. G* **28** (2002) 2693, doi:10.1088/0954-3899/28/10/313.